Targeting the MET oncogene by concomitant inhibition of receptor and ligand via an antibody-"decoy" strategy

Targeting the *MET* oncogene by concomitant inhibition of receptor and ligand via an antibody-'decoy' strategy

Cristina Basilico[1*], Chiara Modica[1,2*], Federica Maione[1], Elisa Vigna[1,2 §] and Paolo M Comoglio[1§]

[1] Candiolo Cancer Institute, FPO-IRCCS, Strada Provinciale 142, 10060 Candiolo (TO), Italy

[2] Department of Oncology, University of Turin

[*]Cristina Basilico and Chiara Modica contributed equally to this work

[§]Elisa Vigna and Paolo M Comoglio share senior authorship of this work

Corresponding author: Cristina Basilico, Laboratory of Molecular Therapeutics and Exploratory Research, Candiolo Cancer Institute, FPO-IRCCS, Strada Provinciale 142, 10060 Candiolo (TO), Italy. Tel: +39 011 9933228; Fax: +39 011 9933225; e-mail: cristina.basilico@ircc.it

Category: Cancer Therapy and Prevention

Short title: Vertical inhibition of the HGF/MET axis.

Keywords: *MET* oncogene, antibodies, decoy, MET target therapy, anti-HGF therapy

Abbreviations: HGF, Hepatocyte Growth Factor; IPT domain, Ig-like, Plexin, Transcription factor domain; hHGF-Ki mice, human Hepatocyte Growth Factor Knock-in mice; MFI, Mean Fluorescence Intensity.

Novelty and impact: In a large number of cancer patients, HGF-induced MET signaling is exploited by tumor cells as an 'expedient' to boost the malignant phenotype and to engender drug resistance. We developed a new strategy aimed at concomitant targeting of a ligand and a receptor belonging to the same axis. This paper addresses the unmet medical need to treat tumors in the absence of MET genetic lesions, a condition in which cancer cells are barely sensitive to MET inhibitors. These results may have implications for clinical trials.

Abstract

MET, a master gene sustaining 'invasive growth', is a relevant target for cancer precision therapy. In the vast majority of tumors, wild-type *MET* behaves as a 'stress-response' gene and relies on the ligand (HGF) to sustain cell 'scattering', invasive growth and apoptosis protection (oncogene *'expedience'*). In this context concomitant targeting of MET and HGF could be crucial to reach effective inhibition. To test this hypothesis, we combined an anti-MET antibody (MvDN30) inducing '*shedding*' (*i.e.* removal of MET from the cell surface), with a '*decoy*' (*i.e.* the soluble extracellular domain of the MET receptor) endowed with HGF-sequestering ability. To avoid antibody/decoy interaction -and subsequent neutralization- we identified a single aminoacid in the extracellular domain of MET -lysine 842- that is critical for MvDN30 binding, and engineered the corresponding recombinant decoyMET (K842E). DecoyMET^{K842E} retains the ability to bind HGF with high affinity and inhibits HGF-induced MET phosphorylation. In HGF-dependent cellular models, MvDN30 antibody and decoyMET^{K842E} used in combination cooperate in restraining invasive growth, and synergize in blocking cancer cell '*scattering'*. The antibody and the decoy unbridle apoptosis of colon cancer stem cells grown *in vitro* as spheroids. In a preclinical model, built by orthotopic transplantation of a human pancreatic carcinoma in SCID mice engineered to express human HGF, concomitant treatment with antibody and decoy significantly reduces metastatic spread. The data reported indicate that vertical targeting of the MET/HGF axis results in powerful inhibition of ligand-dependent MET activation, providing proof of concept in favor of combined target therapy of MET '*expedience'*.

Introduction

Metastatic spreading is based on the ability of cancer cells to disrupt cell-to-cell interactions, migrate through the extracellular matrix, survive and proliferate in tissues other than their site of origin. The physiological counterpart of this complex program – known as 'invasive growth' – is at the basis of embryogenesis and accounts for wound healing and organ regeneration during adult life. Invasive growth is tightly regulated by specific extracellular signals, one of which is Hepatocyte Growth Factor (HGF), the ligand for the receptor encoded by *MET* oncogene[1]. In conditions of aberrant activation, HGF/MET signaling drives tumor onset, progression and metastasis in a broad spectrum of human malignancies[2]. In a minority of events, *MET* behaves as a 'driver' oncogene and tumor cells are dependent on constitutive MET signaling for growth and survival ('*MET addiction'*). This condition relies on the presence of genetic lesions, mostly increased gene copy number[3, 4] or -less frequently- mutations[5], that result in constitutive ligand-independent receptor activation. In this context, treatment with MET inhibitors is highly effective, inducing block of cell proliferation and cell cycle arrest *in vitro* and inhibition of tumor growth *in vivo*[6, 7]. The co-expression of ligand and receptor within the same cell is another strategy exploited by cancer to achieve continuous MET activation, and has been described mainly in non-epithelial human cancers, such as osteosarcomas[8], glioblastomas[9] and multiple myelomas[10]. In most cases, however, aberrant MET activation in tumors originates from receptor over-expression, due to transcriptional upregulation of the wild-type gene, triggering cancer cell sensitization to ligand stimulation[11]. In the latter case, MET signaling –which results in pro-invasive and anti-apoptotic responses– is exploited by cancer cells as a strategy to bypass stress conditions and boosts the malignant phenotype ('*MET expedience'*[12]). In the absence of specific genetic lesions, *MET* is not strictly necessary for tumor growth, but the presence of the ligand sustains receptor activation, enhancing the malignant phenotype. Finally, MET behaves as a functional marker of cancer 'stem-progenitor' cells in glioblastomas[13, 14], and supports the 'stem' phenotype in colorectal and breast cancers[15, 16]. Moreover, it has been shown that stromal-derived HGF sustains the WNT self-renewal pathway of colorectal cancer stem cells and promotes proliferation of colon cancer initiating cells, triggering resistance to anti-EGFR therapy[17].

A number of strategies targeting MET or HGF –either small molecule inhibitors, antibodies or recombinant proteins- have been designed and are currently under investigation[18, 19]. Among them, the MvDN30 antibody is a monovalent chimeric Fab fragment that binds to the extracellular domain of MET, inducing proteolytic cleavage ('*shedding*') of the receptor from the cell surface[20]. DecoyMET is a recombinant soluble receptor encompassing the whole extracellular region of MET; it binds HGF with high affinity and inhibits ligand-driven biological activities *in vitro* and *in vivo* when expressed by lentiviral vector technology[21] or as Fc-fusion protein[22, 23]. MvDN30 and decoyMET, used in combination, would allow dual targeting of ligand and receptor, acting simultaneously on MET-expressing cancer cells and on HGF-secreting tumor stroma. We show that vertical inhibition of the MET/HGF axis effectively hinders tumor cell growth, motility and invasion *in vitro* and significantly reduces metastatic spreading *in vivo*, providing proof of concept for combined targeted therapy in a broad spectrum of cancers expressing wild-type MET.

Materials and methods

Cell culture

A549 human lung adenocarcinoma cells, HPAF-II human pancreatic adenocarcinoma cells and U87-MG human glioblastoma cells were obtained from ATCC/LGC Standards S.r.l. (Sesto San Giovanni, Italy) and cultured as suggested by the supplier. Human metastatic colorectal cancer M049 spheroid cultures (courtesy of Carla Boccaccio, University of Torino) were maintained as described[15]. M049 three dimensional cultures were established by mechanical disaggregation of xenopatient tumors, embedded in Growth Factor Reduced Matrigel (Corning) and cultured as described[15] with the addiction of 2 µM N-acetyl-L-cysteine (Sigma). All cell cultures were tested for mycoplasma contamination.

Generation, expression and purification of mutated MET ectodomains

cDNA sequences of human MET ectodomains (decoyMET) carrying single aminoacid substitutions were generated using the QuickChange II Site-Directed Mutagenesis Kit (Agilent Technologies, Santa Clara, CA). Engineered soluble receptors were produced by transient transfection of HEK-293T cells with pcDNA3.1 plasmids (Invitrogen Corporation, Camarillo, CA)

expressing cDNAs encoding for wild-type decoyMET or decoyMET mutants, and purified from cell supernatants by affinity chromatography using HisTrap HP columns (GE Healthcare, Freiburg, Germany) according to manifacturer's instructions. Large-scale protein production and purification were performed by U-Protein Express BV (Utrecht, The Netherlands).

Generation of a tridimensional homology model

The homology model was built by alignment of MET IPT 3-4 domains (wild-type and mutated) with the crystal structure of the top scored homologous Plexin A1 domains 7-10, IPT3-IPT6 (PDB 5L7N)24 using SWISS-MODEL software (www.swissmodel.expasy.org).

Immunoprecipitation assays

To analyze the interaction of wild-type decoyMET or decoyMET mutants with anti-MET antibodies, comparable amounts of decoyMET proteins -obtained from cells supernatants as described above and normalized according to Western blot analysis- were incubated with DN30 or DO24 monoclonal antibodies[25] for 30 minutes at 4°C. Antibody-decoyMET complexes were immunoprecipitated with Sepharose-Protein A (GE Healthcare Life Science) and revealed by Western blot using HRP-conjugated streptactin (IBA, Goettingen, Germany). Signal was detected using ECL System (GE Healthcare). To analyze the interaction of wild-type decoyMET or decoyMET^{K842E} with HGF, comparable amounts of decoyMET proteins, obtained and normalized as above, were mixed with 1 ml of supernatants from MDA-MB-435 cells transduced with a Lentiviral vector expressing human HGF[26] or supernatants from untransduced cells. After 2 h incubation at 4°C, the complexes were immunopreciptated with DO24 immobilized on Sepharose-Protein A and revealed by Western blot using the biotinylated anti-HGF antibody BAF294 (R&D Systems, Minneapolis, MN) followed by decoration with HRP-conjugated streptavidin (GE Healthcare). Signal was detected using ECL System (GE Healthcare).

MET phosphorylation assay

Serum-starved A549 cells were incubated for 24 h with 125 nM MvDN30 or 2 µM decoyMET^{K842E}, alone or in combination, and then stimulated with 50 ng/ml HGF (R&D Systems) for 2 h at 4°C. Total cellular lysates were analyzed by Western blot using the following primary antibodies: anti-MET phospho-Tyr$^{1234/1235}$ (D26, Cell Signaling Technology, Beverly, MA); anti-MET (3D4, Invitrogen Corporation); anti-vinculin (clone hVIN-1, Sigma, Saint Louis, MO).

Secondary HRP-conjugated anti-mouse or anti-rabbit IgGs were from Jackson Immuno Research (West Grove, PA). Western blot bands were quantified with ImageJ software. PhosphoMET signal was normalized on vinculin (loading control. Values obtained were converted in logarithmic form, control (HGF-treated sample) subtracted, and represented with heatmaps generated by the freeware Gedas program[27].

Phosphorylation of downstream transducers

Serum-starved A549 cells were incubated for 24 h with 500 nM MvDN30 or 2 μM decoyMETK842E, alone or in combination, and then stimulated with 100 ng/ml HGF (R&D Systems) for 15 min at 37°C. Total cellular lysates were analyzed by Western blot using the following primary antibodies: anti-ERK phospho-Thr202/Tyr204 (Cell Signaling Technology); anti-ERK (Cell Signaling Technology); anti-AKT phospho-Ser473 (Cell Signaling Technology); anti-AKT (Cell Signaling Technology); anti-GAPDH (D4C6R, Cell Signaling Technology). Secondary HRP-conjugated anti-mouse or anti-rabbit IgGs were from Jackson Immuno Research. Western blot bands were quantified with ImageJ software. PhosphoERK and phosphoAKT were normalized on the corresponding total proteins. Heatmaps were generated as described above.

ELISA Binding Assays

For analysis of the interaction between decoyMET and the DN30 or DO24 mAbs, affinity-purified soluble receptors (wild-type decoyMET or decoyMET^{K842E}, 100 ng/well) were immobilized on ELISA plates and increasing concentrations of the antibodies (0 – 100 nM) were added in liquid phase. Binding was revealed using HRP-conjugated anti-mouse antibodies (GE Healthcare). For analysis of decoyMET binding to HGF, soluble receptors (50 ng/well) were immobilized on ELISA plates pre-coated with the DO24 antibody (100 ng/well) and incubated with increasing concentrations of HGF (0-10 nM) in solution. Binding was detected using the anti-HGF biotinylated antibody BAF294 (R&D Systems) and revealed with HRP-conjugated streptavidin (GE Healthcare). Colorimetric assay was quantified by the multi-label plate reader VICTOR-X4 (Perkin Elmer Instruments INC., Whaltman, MA). Data were analyzed and fit using Prism software (GraphPad).

***In vitro* biological assays**

For anchorage-independent growth assays, cells were suspended in the appropriate culture medium supplemented with 2% FBS and 0.5% Seaplaque agarose (BMA, Rockland, ME), and seeded in 48-well plates (500 cells/well) on top of 1% agarose. Fresh medium containing the treatments was supplied twice weekly. A549 cells were treated with 1 μM MvDN30 or 1 μM decoyMET^{K842E}, alone or in combination, in the presence of 30 ng/ml HGF. U87-MG cells were treated with 0.5 μM MvDN30 or 1 μM decoyMET^{K842E}, alone or in combination. Colonies were stained with tetrazolium salts (Sigma) after 12 days of culture. Colony growth was determined using Metamorph software (Molecular Devices, Sunnyvale, CA). For cell invasion assays, HPAF-II cells (1.5 X 10^5/well) were suspended in serum-free culture medium in the presence of 0.5 μM MvDN30 or 1 μM decoyMET^{K842E}, alone or in combination, and seeded on the upper compartment of transwell chambers pre-coated with 30 μg/well of Matrigel Matrix (Corning Incorporated, NY). Culture medium supplemented with 2% FBS and 12.5 ng/ml HGF was added to the lower compartment of the chamber. After 24 h, cells on the upper side of the transwell filters were mechanically removed, while cells migrated through the membrane were fixed with 11% glutaraldehyde and stained with 0.1% Crystal Violet. Cell invasion was quantified with Image-J software. For cell scattering assays, HPAF-II cells (8000/well) were seeded in 96-well plates in complete culture medium. After 6 h, increasing concentrations (0 - 4 μM) of MvDN30 or decoyMET^{K842E}, alone or in 1:1 combination, were added. After additional 24 h, cells were stimulated with 6.25 ng/ml HGF for 20 h. Cells were fixed with 11% glutaraldehyde and stained with 0.1% Crystal Violet (Sigma-Aldrich). For real-time cell motility assay, HPAF-II cells were seeded in E-plates (8000/well; Roche Diagnostics, Mannheim, Germany) and treated as above. Electrical impedance was monitored continuously for 48 h, with data recording every ten minutes, using a X-Celligence RTCA device (Roche Diagnostic). Values are expressed as cell index normalized at the instant of HGF addition. For viability assays, spheroids were seeded in 96-well plates (1000/well) in stem cell medium in the presence of 20 ng/ml HGF. The following day, spheroids were treated with increasing concentrations of MvDN30 or decoyMET^{K842E} (0 - 700 nM), either alone or in 1:1 combination. After 4 days of treatment, cell number was determined using CellTiter-Glo (Promega Corp., Madison, WI) with a VICTOR X4 multi-label plate reader (Perkin Elmer). Data were analyzed and fit using Prism software (GraphPad). For apoptosis assays, spheroids were seeded as above and treated with 77 nM MvDN30 and 25 nM

decoyMET^{K842E} in the presence of 20 ng/ml HGF. Apoptosis was determined after 48 h by the free nucleosome method using a Cell Death Detection ELISA^{PLUS} Kit (Roche diagnostics).

Immunofluorescence

Immunofluorescence analysis on tumor cells and tissues was performed as described[28, 29]. Staining was done with: anti-MET phospho-Tyr$^{1234/1235}$ primary antibody (D26) revealed by Alexa Fluor 555-conjugated secondary antibody; anti-E-cadherin primary antibody (EP700Y, Abcam, Cambridge, UK) revealed by Alexa Fluor 488-conjugated secondary antibody; anti-vimentin primary antibody (VIM 3B4, Merk. Vimodrone, Italy) revealed by Alexa Fluor 555-conjugated secondary antibody; anti-cleaved Caspase-3 (Asp175) primary antibody (Cell Signaling Technology) revealed by Alexa Fluor 488-conjugated secondary antibody. Cells were counterstained with 488-conjugated phalloidin (Molecular Probes, USA). All images were captured with a Leica TCS SP5 AOBS confocal laser-scanning microscope (Leica Microsystems). Immunofluorescence acquisition settings were kept constant within each cell line or tumor tissue. Mean Fluorescence Intensity (MFI) was evaluated with ImageJ software, measuring the mean pixel intensity in each channel, background subtracted. MFI was normalized on phalloidin for cell lines and spheroids and on DAPI for tumors.

***In vivo* experiments**

All animal procedures were performed according to protocols approved by Ethical Committee for animal experimentation of the Fondazione Piemontese per la Ricerca sul Cancro and by Italian Ministry of Health. NOD-SCID mice were purchased from Charles River (Calco, Italy); hHGF-Ki SCID mice were obtained from AVEO Pharmaceuticals, Cambridge, MA. U87-MG cells were injected subcutaneously (2x106/mouse) in the right flank of female NOD-SCID mice. Tumor growth was monitored by caliper measurement twice weekly and tumor volume was calculated as previously described30. When the tumors reached a volume of 80-100 mm3 (day 0), mice were stratified in four homogeneous groups and treated twice weekly by intratumor injection with: vehicle (n=10); MvDN30, 12.5 µg (n=9); K842E, 125 µg (n=9); the combination of the two (n=10). After 22 days of treatment, mice were sacrificed and tumors were excised and embedded in paraffin for histological analysis. Tumor volume fold increase is calculated as the ratio between the value at day 22 and the one at day 0. HPAF-II cells were transduced with 100 ng/ml p24 of lentiviral vectors carrying the luciferase gene under the control of the CMV

promoter as described[31]. Luciferase-expressing HPAF-II cells (10^4/mouse) were injected in the pancreas of 4- to 6-week-old female hHGF-Ki SCID mice. After two days, mice were injected intraperitoneally with XenoLight D-Luciferin (150 mg/kg; Perkin Elmer), stratified into homogeneous groups on the basis of the bioluminescence signal using an IVIS Spectrum CT apparatus (Perkin Elmer), and randomly assigned to 4 treatment arms: vehicle (*n*=10); MvDN30 (10 mg/kg, *n*=6); decoyMET^{K842E} (10 mg/kg, *n*=6); MvDN30 + decoyMET^{K842E} (10 + 10 mg/kg , *n*=6). Treatments were administered daily (MvDN30) or every two days (decoyMET^{K842E}) by intraperitoneal injection. At sacrifice, after five weeks of treatment, tumors and lungs were excised. Tumors were embedded in paraffin or OCT and processed for immunohistochemical or immunofluorescence analysis, respectively. Proliferation of tumor cells was determined using a monoclonal anti-Ki67 antibody (MIB-1, Agilent Technologies) as previously described[32]. Lungs were processed for histochemical analysis and micrometastases were evaluated by light microscopy on paraffin-embedded, HE-stained non sequential sections. For each mouse, ten slides were analyzed; metastatic lesions were scored and their area quantified with ImageJ software.

Statistical analysis

Average, standard deviation (SD) and standard error of the mean (SEM) were calculated using Microsoft Office Excel 2010 software (Microsoft Corporation, Redmond, Washington). To calculate K_d values, data from ELISA assays were analyzed and fitted according to nonlinear regression, one site binding hyperbola curve, using GraphPad Prism software (GraphPad Software, San Diego, California). To calculate IC_{50} values, data from proliferation assays were analyzed and fitted according to nonlinear regression, sigmoidal dose-response curve, using GraphPad Prism software. Statistical significance was determined using a two-tailed Student's *t* test. All experiments were repeated at least three times. The *in vivo* experiments were performed two times. Figures show one representative experiment.

Results

Site-directed mutagenesis of the DN30-binding epitope in decoyMET

To exploit the activity of MvDN30 antibody and decoyMET in combination, it is mandatory to prevent interaction between the two molecules, that would result in mutual neutralization. It has been shown previously that MvDN30 recognizes an epitope within the IPT-4 domain of MET extracellular region at the boundary with the IPT-3 domain[33]. Former studies showed that the parental DN30 antibody, that binds the human receptor with picomolar affinity, also interacts with dog and rat MET[25, 34], while it does not cross-react with mouse[20]. Upon alignment of the IPT-3 and IPT-4 aminoacid sequences of the above-mentioned mammalian species, a number of residues were identified that are selectively changed in the mouse (Fig. 1A). To test if human-to-mouse swapping of single aminoacid residues could impair antibody binding, soluble receptors carrying point mutations in the IPT 3-4 domain were generated and tested against the DN30 antibody. Substitution of lysine 842 with glutamic acid generated decoyMET^{K842E}, a modified soluble receptor not recognized anymore by the antibody, while all other mutations did not affect the interaction (Fig. 1B). This mutation did not disrupt the overall structure of the protein, in fact decoyMET^{K842E} was immunoprecipitated by DO24, an antibody binding a different epitope in the extracellular region of MET[25] (Fig. 1C). This result was confirmed in ELISA assays, performed with affinity-purified decoys in solid phase and antibodies in liquid phase (Fig. 1D). The homology model of the IPT 3-4 domains shows that the residue at position 842 is exposed at the surface. The substitution of lysine with glutamic acid induces an evident structural modification, presumably resulting in critical perturbation of the binding site and thus hampering decoyMETK842E-antibody interaction (Fig. 1E).

DecoyMET^{K842E} binds HGF with high affinity

We then investigated if the K842E amino acid substitution interferes with binding of HGF. In immunoprecipitation assays, the amount of HGF bound by decoyMET^{K842E} was comparable or higher to the amount bound by wild-type decoyMET (Fig. 2A). In ELISA binding assays, the affinity constant of decoyMET^{K842E} for HGF (K_d = 1.04 ± 0.05 nM) was superimposable with the K_d of 1.44 ± 0.07 nM measured for the wild-type decoyMET (Fig. 2B). Finally, the inhibitory activity of decoyMET^{K842E} was tested in an HGF-induced MET phosphorylation assay. As shown

in Fig. 2C, wild-type decoyMET and decoyMET^{K842E} inhibited HGF-dependent MET phosphorylation in A549 lung cancer cells with comparable potency. Thus, the K842E substitution does not interfere with the formation of a stable complex with HGF, and leaves the inhibitory activity of the decoy unaffected.

MvDN30 and decoyMET^{K842E} cooperate in inhibition of MET phosphorylation and downstream biological responses

To assess the inhibitory activity elicited by concomitant targeting of the ligand and the receptor on MET signal transduction, we tested MET phosphorylation in the presence of MvDN30 and decoyMET^{K842E}, either alone or in combination. To this end A549 cells, expressing a wild-type MET receptor, were stimulated with nanomolar concentrations of HGF and MET activation was measured by phosphoMET antibodies. Both molecules displayed inhibitory activity, and the combination of the two was more efficient (Fig. 3A). Analysis of downstream signaling transducers confirmed that the combination achieved the most effective inhibition of ERK and AKT activation (Fig. 3B).

On the biological ground, MvDN30 and decoyMET^{K842E} in combination strongly inhibited anchorage-independent colony growth in cellular models of either autocrine or paracrine HGF stimulation. In the former, U87-MG glioblastoma cells -displaying very efficient colony growth in soft agar due to a MET/HGF autocrine loop- were inhibited by 75% when MvDN30 and decoyMET^{K842E} were used in combination, while colony growth inhibition never exceeded 40% when the two molecules were used as single agents (Fig. 3C). Likewise, the combo treatment completely blocked the formation of A549 soft agar colonies induced by nanomolar concentrations of exogenously-administered HGF, while MvDN30 and decoyMETK842E alone achieved a partial though significant inhibition of colony growth (65% and 74%, respectively, Fig. 3D). Similar results were obtained in invasion assays performed in Matrigel-coated chambers: MvDN30 and decoyMETK842E in combination reduced HGF-driven invasion of HPAF-II human pancreatic adenocarcinoma cells by 85%, while as single agents achieved only 59% and 52% inhibition, respectively (Fig. 3E). In all these biological systems, MvDN30 and decoyMET^{K842E} combination impaired MET phosphorylation more efficaciously than the single treatments (Suppl. Fig. 1).

To assess if the effect of the two inhibitors is additive or synergistic, a quantitative motility assay was performed. HPAF-II human pancreatic adenocarcinoma cells, expressing wild-type

MET, were induced to scatter by HGF. Cell scattering was quantified by measuring the variations of electrical impedance of cell-covered electrodes (X-CELLigence Real Time Cell Analyzer). The two molecules in combination reduced HGF-dependent cell scattering in dose-dependent fashion, starting inhibition at 250 nM and achieving complete blockage in the micromolar range (Fig. 4 A and B). The Cell Index values measured at the end of the experiment (time = 48h) were normalized on HGF (Fig. 4C) and elaborated with the CalcuSYN software to assess synergism (Fig. 4D): for all concentrations examined, the calculated Combination Index (CI) was well below 0.5 (CI = 0.1, 0.09, 0.17 and 0.38 for 0.06, 0.25, 1 and 4 μM, respectively), indicating that MvDN30 and decoyMET^{K842E} display a synergistic behavior[35].

MvDN30 and decoyMET^{K842E} impair growth and survival of colon-derived spheroids

It has been reported that HGF-induced MET activation in colorectal cancer stem cells supports the stem phenotype. Moreover, microenvironmental growth factors -including HGF- play a role in reducing the sensitivity of cancer-derived stem cells to targeted therapies[36]. Colon spheroids -enriched in cancer stem/progenitor cells expressing wild-type MET- were prepared from a patient-derived xenograft of colorectal cancer liver metastasis[15] and tested for growth or apoptosis in the presence of exogenous HGF. In the growth assay, the combination of MvDN30 and decoyMET^{K842E} reached the inhibitory effect (IC_{50}) at concentrations six to eight times lower than the IC_{50} obtained by single treatments (Fig. 5A). In line with these results, treatment by either reagent alone was virtually ineffective in inducing programmed cell death at the dose tested, while a strong pro-apoptotic effect was generated by the concomitant administration of the two molecules (Fig. 5B). Accordingly, the strongest inhibition of HGF-induced MET-phosphorylation was obtained by the combined treatment (Fig. 5C).

MvDN30 and decoyMET^{K842E} attenuate the invasive phenotype and reduce metastatic spread

The inhibitory activity of MvDN30 and decoyMETK842E in combination was assessed in vivo in mouse models of ligand-driven MET stimulation.

The U87-MG glioblastoma xenograft tumor model of autocrine HGF stimulation was investigated. Cells were injected subcutaneously in NOD-SCID mice; when tumors reached a volume of 80-100 mm3, mice were stratified in homogeneous groups and randomly assigned to 4 treatment arms: Vehicle, MvDN30, decoyMETK842E or the combination of the two. After 22 days of treatment, mice were sacrificed and primary tumors excised for histological

examination. While the combo treatment induced only a marginal inhibition of growth, reduction of phenotypic hallmarks of tumor invasion was observed (Suppl Fig.2).

The combo treatment was also challenged in a paracrine model of HGF stimulation. As previously reported, mouse HGF does not activate the human MET receptor[37, 38]. Hence, to test the inhibitory activity of decoyMET^{K842E} in xenografts of human tumors, we exploited a transgenic SCID mouse where the mouse HGF gene was replaced by the human gene (hHGF-Ki)[39]. Human pancreatic adenocarcinoma cells (HPAF-II) were labeled by transduction with the luciferase gene and injected orthotopically in the pancreas of hHGF-Ki mice. Engraftment was checked by analysis of total body luminescence; mice were stratified into homogeneous groups on the basis of bioluminescence values, and randomly assigned to 4 treatment groups: VEHICLE, MvDN30, decoyMET^{K842E} or the combination of the two. Tumor growth was monitored by total body luminescence (Suppl. Fig. 3A). At sacrifice, 5 weeks after cell injection, tumors were excised and analyzed for MET phosphorylation, proliferation, apoptosis and vimentin/E-cadherin expression (markers of epithelial-mesenchimal transition). Concurrently, lungs were collected for histochemical evaluation of metastatic nodules. The phosphorylated status of MET at Tyrosines 1234-1235 was inhibited by either agents, and the combo treatment elicited a dramatic effect (Fig. 6A). As expected in this model of MET oncogene 'expedience' (i.e. expression of wild-type MET), proliferation as well as apoptosis were modestly affected, and only by the combo treatment (Suppl. Fig. 3B and C). Analysis of the ratio between vimentin and E-cadherin showed that the combination treatment pushed cancer cells towards a more epithelial phenotype (Fig. 6B). Accordingly, concomitant administration of MvDN30 and decoyMETK842E significantly inhibited MET-driven metastatic dissemination to the lung (Fig. 6C).

Discussion

Pharmacological inhibition of the MET tyrosine kinase receptor in oncogene 'addicted' cancer cells extinguishes cell proliferation and invasion. Accordingly, patients with *MET* amplified advanced Non-Small Cell Lung Cancer (NSCLC), metastatic gastric or esophageal cancer respond to anti-MET therapy[40,41]. On the other hand, cancer cells without *MET* genetic alterations exploit the 'physiological' program triggered by the oncogene as an 'expedient' to boost the malignant phenotype. *'Expedience'* requires stimulation of wild-type MET by its ligand HGF. In this respect, the contribution of tumor microenvironment to cancer progression and metastasis is becoming increasingly relevant, as experimental evidences suggest that the malignant phenotype does not develop in a strictly cell-autonomous way, but in a rather complex interplay between cancer cells and host stroma[42]. The tumor microenvironment is a significant source of HGF, secreted by stromal cells of mesenchymal origin as an inactive precursor (proHGF). The latter is stored in the extracellular matrix, thanks to its avidity for heparansulfates, and is activated by specific proteases produced either by tumor or stromal cells[43]. Therefore, an excess of biologically active ligand is readily available for binding the MET receptor and triggers the invasive growth signaling cascade in 'non-addicted' cells. This paper shows that in conditions of *MET 'expedience'*, a concomitant intervention hitting both sides of the MET/HGF axis results in improved inhibitory activity. Simultaneous targeting was achieved combining a monovalent MET antibody, MvDN30, with a recombinant soluble receptor, decoyMET^{K842E}. The data provided herein indicate that there is no redundancy in targeting the same pathway with complementary tools. We selected the two inhibitors on the basis of their mechanisms of action. The antibody induces the physical removal of MET from the cell surface by 'shedding' of the ectodomain; the latter is released in the extracellular environment and acts as 'decoy' for HGF. Exogenous supply of recombinant decoyMET reinforces the HGF-sequestering activity of the endogenous decoyMET generated by MvDN30. To enable the concomitant use of MvDN30 and decoyMET, a modified soluble receptor was generated (decoyMET^{K842E}), deficient in MvDN30 interaction but endowed with high affinity binding properties to HGF. The two agents in combination cooperate in a variety of cancer cells, reducing the effective therapeutic dose. Moreover, this 'dual strategy' displays a strong synergistic effect, potentially exerting a superior anti-tumor efficacy. Interestingly, the

combination of MvDN30 and decoyMET^{K842E} impairs growth and survival of patient-derived colon cancer stem cells expressing MET. MET expression in a sub-population of stem/progenitor cancer cells has been defined as *MET 'inherence'*[44], *i.e.* the physiologic (inherent) HGF-induced intracellular response activated in cancer stem cells - in the absence of genetic lesions- responsible for resistance to targeted therapies, such as Epidermal Growth Factor Receptor (EGFR) inhibitors in colorectal cancer. The notion linking cancer stem cells and resistance to conventional therapies is largely accepted, and the role of microenvironmental HGF in maintaining the stem phenotype of MET-expressing progenitor cells is becoming more and more established. An effective anti-MET treatment, as the combination of MvDN30 and decoyMET^{K842E}, could represent a therapeutic support to blunt cancer stem cells and to oppose the onset of resistance to targeted therapies. On the other hand, in all cases where MET activation is ligand-independent -i.e. in the presence of activating mutations, occurring in solid tumors with a frequency of 1-2% (COSMIC database: www.sanger.ac.uk)- the vertical inhibition of the MET/HGF axis may be redundant.

The role of host microenvironment is difficult to investigate in mouse xenografts due to the limited cross-reactivity between murine stromal-derived factors and specific targets on human cancer cells. This is particularly significant in the case of the HGF/MET system, because murine HGF does not activate human MET[37, 38]. The development of genetically modified mouse strains expressing the Knocked-in human HGF gene (hHGF-Ki mice) circumvented this problem. In this transgenic model, we show that concomitant targeting of environmental HGF and its receptor on cancer cells may be an effective therapeutic strategy to hinder malignant progression and metastasis.

Xenografts of pancreatic adenocarcinoma are characterized by precocious metastatic dissemination, occurring very early during tumor development, and are sustained by an abundant stromal compartment[45,46]. Recently, HGF secreted by pancreatic stellate cells was identified as a factor playing a relevant function in tumor-stroma interaction in this type of malignancy[47]. In an orthotopic mouse model of human pancreatic adenocarcinoma grafted in hHGF-Ki mice, MvDN30 and decoyMET^{K842E} in combination slightly delayed tumor growth, as expected in a model of *'expedience'* where *MET* is not the driver oncogene. On the other hand, the combo treatment proved to be very effective in reducing the metastatic spread, suggesting a possible therapeutic application in non-addicted cancer cells featuring wild-type MET.

Epidemiological data show that only 2-3% of epithelial cancers rely on *MET* oncogenic addiction, either because of gene amplification, rearrangement or mutation (COSMIC database: www.sanger.ac.uk). For this reason, a number of clinical trials -addressing unselected populations of cancer patients- failed[48, 49]. On the other hand, the vast majority of carcinomas exploit ligand-dependent wild-type MET activation to unleash the invasive metastatic phenotype in response to hypoxia, ionizing radiation or chemotherapy[50-52]. Thus these findings suggest that a large cohort of patients -currently unfit to MET targeted therapy due to the absence of a specific genetic lesion- should benefit from treatments inspired by the dual antibody-decoy strategy, that allows optimal blockade of the HGF-driven MET signaling.

Acknowledgments

We thank Paolo Luraghi for supplying colon cancer spheroids and AVEO Pharmaceuticals for providing hHGF-Ki/SCID mice, Carla Boccaccio for advices and criticism, Letizia Lanzetti for helpful scientific discussion, Cristina Chiriaco and Lara Fontani for support in the *in vitro* experiments, Federica Di Nicolantonio for help in drug combination analysis, and Stefania Giove for skilled technical assistance. This work was supported by AIRC IG, Project no 15572; AIRC Special Program 5xMille 2010 MCO, Project no 9970; grant FPRC 5xMille Ministero della Salute 2013; grant FPRC 5xMille Ministero della Salute 2014 to PMC. Paolo M Comoglio and Elisa Vigna are authors of the international patent W02007090807 ('Anti-met monoclonal antibody, fragments and thereof…') owned by Metis Precision Medicine SB (Italy), and co-founders of Metis Precision Medicine SB. Paolo M Comoglio is also co-founder of Octimet Oncology NV. Both companies did not interfere in the design of the study, analysis of data and decision to publish.

References

1. Trusolino L, Comoglio PM. Scatter-factor and semaphorin receptors: cell signalling for invasive growth. *Nat Rev Cancer* 2002;**2**: 289-300.

2. Birchmeier C, Birchmeier W, Gherardi E, Vande Woude GF. Met, metastasis, motility and more. *Nat Rev Mol Cell Biol* 2003;**4**: 915-25.

3. Lutterbach B, Zeng Q, Davis LJ, Hatch H, Hang G, Kohl NE, Gibbs JB, Pan BS. Lung cancer cell lines harboring MET gene amplification are dependent on Met for growth and survival. *Cancer Res* 2007;**67**: 2081-8.

4. Smolen GA, Sordella R, Muir B, Mohapatra G, Barmettler A, Archibald H, Kim WJ, Okimoto RA, Bell DW, Sgroi DC, Christensen JG, Settleman J, et al. Amplification of MET may identify a subset of cancers with extreme sensitivity to the selective tyrosine kinase inhibitor PHA-665752. *Proc Natl Acad Sci U S A* 2006;**103**: 2316-21.

5. Schmidt L, Duh FM, Chen F, Kishida T, Glenn G, Choyke P, Scherer SW, Zhuang Z, Lubensky I, Dean M, Allikmets R, Chidambaram A, et al. Germline and somatic mutations in the tyrosine kinase domain of the MET proto-oncogene in papillary renal carcinomas. *Nat Genet* 1997;**16**: 68-73.

6. Bardelli A, Corso S, Bertotti A, Hobor S, Valtorta E, Siravegna G, Sartore-Bianchi A, Scala E, Cassingena A, Zecchin D, Apicella M, Migliardi G, et al. Amplification of the MET receptor drives resistance to anti-EGFR therapies in colorectal cancer. *Cancer Discov* 2013;**3**: 658-73.

7. McDermott U, Sharma SV, Dowell L, Greninger P, Montagut C, Lamb J, Archibald H, Raudales R, Tam A, Lee D, Rothenberg SM, Supko JG, et al. Identification of genotype-correlated sensitivity to selective kinase inhibitors by using high-throughput tumor cell line profiling. *Proc Natl Acad Sci U S A* 2007;**104**: 19936-41.

8. Ferracini R, Di Renzo MF, Scotlandi K, Baldini N, Olivero M, Lollini P, Cremona O, Campanacci M, Comoglio PM. The Met/HGF receptor is over-expressed in human osteosarcomas and is activated by either a paracrine or an autocrine circuit. *Oncogene* 1995;**10**: 739-49.

9. Moriyama T, Kataoka H, Koono M, Wakisaka S. Expression of hepatocyte growth factor/scatter factor and its receptor c-Met in brain tumors: evidence for a role in progression of astrocytic tumors (Review). *Int J Mol Med* 1999;**3**: 531-6.

10. Börset M, Hjorth-Hansen H, Seidel C, Sundan A, Waage A. Hepatocyte growth factor and its receptor c-met in multiple myeloma. *Blood* 1996;**88**: 3998-4004.

11. Blumenschein GR, Mills GB, Gonzalez-Angulo AM. Targeting the hepatocyte growth factor-cMET axis in cancer therapy. *J Clin Oncol* 2012;**30**: 3287-96.

12. Comoglio PM, Giordano S, Trusolino L. Drug development of MET inhibitors: targeting oncogene addiction and expedience. *Nat Rev Drug Discov* 2008;**7**: 504-16.

13. De Bacco F, Casanova E, Medico E, Pellegatta S, Orzan F, Albano R, Luraghi P, Reato G, D'Ambrosio A, Porrati P, Patanè M, Maderna E, et al. The MET oncogene is a functional marker of a glioblastoma stem cell subtype. *Cancer Res* 2012;**72**: 4537-50.

14. Joo KM, Jin J, Kim E, Ho Kim K, Kim Y, Gu Kang B, Kang YJ, Lathia JD, Cheong KH, Song PH, Kim H, Seol HJ, et al. MET signaling regulates glioblastoma stem cells. *Cancer Res* 2012;**72**: 3828-38.

15. Luraghi P, Reato G, Cipriano E, Sassi F, Orzan F, Bigatto V, De Bacco F, Menietti E, Han M, Rideout WM, Perera T, Bertotti A, et al. MET signaling in colon cancer stem-like cells blunts the therapeutic response to EGFR inhibitors. *Cancer Res* 2014;**74**: 1857-69.

16. Gastaldi S, Sassi F, Accornero P, Torti D, Galimi F, Migliardi G, Molyneux G, Perera T, Comoglio PM, Boccaccio C, Smalley MJ, Bertotti A, et al. Met signaling regulates growth, repopulating potential and basal cell-fate commitment of mammary luminal progenitors: implications for basal-like breast cancer. *Oncogene* 2013;**32**: 1428-40.

17. Vermeulen L, De Sousa E Melo F, van der Heijden M, Cameron K, de Jong JH, Borovski T, Tuynman JB, Todaro M, Merz C, Rodermond H, Sprick MR, Kemper K, et al. Wnt activity defines colon cancer stem cells and is regulated by the microenvironment. *Nat Cell Biol* 2010;**12**: 468-76.

18. Skead G, Govender D. Gene of the month: MET. *J Clin Pathol* 2015;**68**: 405-9.

19. Vigna E, Comoglio PM. Targeting the oncogenic Met receptor by antibodies and gene therapy. *Oncogene* 2015;**34**: 1883-9.

20. Petrelli A, Circosta P, Granziero L, Mazzone M, Pisacane A, Fenoglio S, Comoglio PM, Giordano S. Ab-induced ectodomain shedding mediates hepatocyte growth factor receptor down-regulation and hampers biological activity. *Proc Natl Acad Sci U S A* 2006;**103**: 5090-5.

21. Michieli P, Mazzone M, Basilico C, Cavassa S, Sottile A, Naldini L, Comoglio P. Targeting the tumor and its microenvironment by a dual-function decoy Met receptor. *Cancer Cell* 2004;**6**: 61-73.

22. Tiran Z, Oren A, Hermesh C, Rotman G, Levine Z, Amitai H, Handelsman T, Beiman M, Chen A, Landesman-Milo D, Dassa L, Peres Y, et al. A novel recombinant soluble splice variant of Met is a potent antagonist of the hepatocyte growth factor/scatter factor-Met pathway. *Clin Cancer Res* 2008;**14**: 4612-21.

23. Coxon A, Rex K, Meyer S, Sun J, Chen Q, Radinsky R, Kendall R, Burgess TL. Soluble c-Met receptors inhibit phosphorylation of c-Met and growth of hepatocyte growth factor: c-Met-dependent tumors in animal models. *Mol Cancer Ther* 2009;**8**: 1119-25.

24. Kong Y, Janssen BJ, Malinauskas T, Vangoor VR, Coles CH, Kaufmann R, Ni T, Gilbert RJ, Padilla-Parra S, Pasterkamp RJ, Jones EY. Structural Basis for Plexin Activation and Regulation. *Neuron* 2016;**91**: 548-60.

25. Prat M, Crepaldi T, Pennacchietti S, Bussolino F, Comoglio PM. Agonistic monoclonal antibodies against the Met receptor dissect the biological responses to HGF. *J Cell Sci* 1998;**111 (Pt 2)**: 237-47.

26. Mazzone M, Basilico C, Cavassa S, Pennacchietti S, Risio M, Naldini L, Comoglio P, Michieli P. An uncleavable form of pro-scatter factor suppresses tumor growth and dissemination in mice. *Journal of Clinical Investigation* 2004;**114**: 1418-32.

27. Fu L, Medico E. FLAME, a novel fuzzy clustering method for the analysis of DNA microarray data. *BMC Bioinformatics* 2007;**8**: 3.

28. Serio G, Margaria V, Jensen S, Oldani A, Bartek J, Bussolino F, Lanzetti L. Small GTPase Rab5 participates in chromosome congression and regulates localization of the centromere-associated protein CENP-F to kinetochores. *Proc Natl Acad Sci U S A* 2011;**108**: 17337-42.

29. Maione F, Capano S, Regano D, Zentilin L, Giacca M, Casanovas O, Bussolino F, Serini G, Giraudo E. Semaphorin 3A overcomes cancer hypoxia and metastatic dissemination induced by antiangiogenic treatment in mice. *J Clin Invest* 2012;**122**: 1832-48.

30. Pacchiana G, Chiriaco C, Stella MC, Petronzelli F, De Santis R, Galluzzo M, Carminati P, Comoglio PM, Michieli P, Vigna E. Monovalency unleashes the full therapeutic potential of the DN-30 anti-Met antibody. *J Biol Chem* 2010;**285**: 36149-57.

31. Amendola M, Venneri MA, Biffi A, Vigna E, Naldini L. Coordinate dual-gene transgenesis by lentiviral vectors carrying synthetic bidirectional promoters. *Nat Biotechnol* 2005;**23**: 108-16.

32. Migliardi G, Sassi F, Torti D, Galimi F, Zanella ER, Buscarino M, Ribero D, Muratore A, Massucco P, Pisacane A, Risio M, Capussotti L, et al. Inhibition of MEK and PI3K/mTOR suppresses tumor growth but does not cause tumor regression in patient-derived xenografts of RAS-mutant colorectal carcinomas. *Clin Cancer Res* 2012;**18**: 2515-25.

33. Vigna E, Chiriaco C, Cignetto S, Fontani L, Basilico C, Petronzelli F, Comoglio PM. Inhibition of ligand-independent constitutive activation of the Met oncogenic receptor by the engineered chemically-modified antibody DN30. *Mol Oncol* 2015;**9**: 1760-72.

34. Gallo S, Gatti S, Sala V, Albano R, Costelli P, Casanova E, Comoglio PM, Crepaldi T. Agonist antibodies activating the Met receptor protect cardiomyoblasts from cobalt chloride-induced apoptosis and autophagy. *Cell Death Dis* 2014;**5**: e1185.

35. Foucquier J, Guedj M. Analysis of drug combinations: current methodological landscape. *Pharmacol Res Perspect* 2015;**3**: e00149.

36. Boccaccio C, Luraghi P, Comoglio PM. MET-mediated resistance to EGFR inhibitors: an old liaison rooted in colorectal cancer stem cells. *Cancer Res* 2014;**74**: 3647-51.

37. Rong S, Oskarsson M, Faletto D, Tsarfaty I, Resau JH, Nakamura T, Rosen E, Hopkins RF, Vande Woude GF. Tumorigenesis induced by coexpression of human hepatocyte growth factor and the human

met protooncogene leads to high levels of expression of the ligand and receptor. *Cell Growth Differ* 1993;**4**: 563-9.

38. Zhang YW, Su Y, Lanning N, Gustafson M, Shinomiya N, Zhao P, Cao B, Tsarfaty G, Wang LM, Hay R, Vande Woude GF. Enhanced growth of human met-expressing xenografts in a new strain of immunocompromised mice transgenic for human hepatocyte growth factor/scatter factor. *Oncogene* 2005;**24**: 101-6.

39. Pennacchietti S, Cazzanti M, Bertotti A, Rideout WM, Han M, Gyuris J, Perera T, Comoglio PM, Trusolino L, Michieli P. Microenvironment-derived HGF overcomes genetically determined sensitivity to anti-MET drugs. *Cancer Res* 2014;**74**: 6598-609.

40. Lennerz JK, Kwak EL, Ackerman A, Michael M, Fox SB, Bergethon K, Lauwers GY, Christensen JG, Wilner KD, Haber DA, Salgia R, Bang YJ, et al. MET amplification identifies a small and aggressive subgroup of esophagogastric adenocarcinoma with evidence of responsiveness to crizotinib. *J Clin Oncol* 2011;**29**: 4803-10.

41. Ou SH, Kwak EL, Siwak-Tapp C, Dy J, Bergethon K, Clark JW, Camidge DR, Solomon BJ, Maki RG, Bang YJ, Kim DW, Christensen J, et al. Activity of crizotinib (PF02341066), a dual mesenchymal-epithelial transition (MET) and anaplastic lymphoma kinase (ALK) inhibitor, in a non-small cell lung cancer patient with de novo MET amplification. *J Thorac Oncol* 2011;**6**: 942-6.

42. Joyce JA, Pollard JW. Microenvironmental regulation of metastasis. *Nat Rev Cancer* 2009;**9**: 239-52.

43. Kawaguchi M, Kataoka H. Mechanisms of hepatocyte growth factor activation in cancer tissues. *Cancers (Basel)* 2014;**6**: 1890-904.

44. Boccaccio C, Comoglio PM. MET, a driver of invasive growth and cancer clonal evolution under therapeutic pressure. *Curr Opin Cell Biol* 2014;**31**: 98-105.

45. Rhim AD, Mirek ET, Aiello NM, Maitra A, Bailey JM, McAllister F, Reichert M, Beatty GL, Rustgi AK, Vonderheide RH, Leach SD, Stanger BZ. EMT and dissemination precede pancreatic tumor formation. *Cell* 2012;**148**: 349-61.

46. Feig C, Gopinathan A, Neesse A, Chan DS, Cook N, Tuveson DA. The pancreas cancer microenvironment. *Clin Cancer Res* 2012;**18**: 4266-76.

47. Pothula SP, Xu Z, Goldstein D, Biankin AV, Pirola RC, Wilson JS, Apte MV. Hepatocyte growth factor inhibition: a novel therapeutic approach in pancreatic cancer. *Br J Cancer* 2016;**114**: 269-80.

48. Spigel DR, Ervin TJ, Ramlau RA, Daniel DB, Goldschmidt JH, Blumenschein GR, Krzakowski MJ, Robinet G, Godbert B, Barlesi F, Govindan R, Patel T, et al. Randomized phase II trial of Onartuzumab in combination with erlotinib in patients with advanced non-small-cell lung cancer. *J Clin Oncol* 2013;**31**: 4105-14.

49. Shah MA, Wainberg ZA, Catenacci DV, Hochster HS, Ford J, Kunz P, Lee FC, Kallender H, Cecchi F, Rabe DC, Keer H, Martin AM, et al. Phase II study evaluating 2 dosing schedules of oral foretinib (GSK1363089), cMET/VEGFR2 inhibitor, in patients with metastatic gastric cancer. *PLoS One* 2013;**8**: e54014.

50. Pennacchietti S, Michieli P, Galluzzo M, Mazzone M, Giordano S, Comoglio PM. Hypoxia promotes invasive growth by transcriptional activation of the met protooncogene. *Cancer Cell* 2003;**3**: 347-61.

51. De Bacco F, D'Ambrosio A, Casanova E, Orzan F, Neggia R, Albano R, Verginelli F, Cominelli M, Poliani PL, Luraghi P, Reato G, Pellegatta S, et al. MET inhibition overcomes radiation resistance of glioblastoma stem-like cells. *EMBO Mol Med* 2016;**8**: 550-68.

52. Avan A, Caretti V, Funel N, Galvani E, Maftouh M, Honeywell RJ, Lagerweij T, Van Tellingen O, Campani D, Fuchs D, Verheul HM, Schuurhuis GJ, et al. Crizotinib inhibits metabolic inactivation of gemcitabine in c-Met-driven pancreatic carcinoma. *Cancer Res* 2013;**73**: 6745-56.

Figure legends

Figure 1. Generation of a mutated decoyMET receptor that does not bind the DN30 antibody.
(A) Comparison of the aminoacid sequences of the third and fourth IPT domains of human, mouse, rat and dog MET. Residues that are changed exclusively in the mouse sequence are highlighted in red, aminoacids that are changed also (or only) in the rat or dog sequences are highlighted in green. Only the IPT-3/IPT-4 boundaries are shown. **(B)** DecoyMET receptors carrying single aminoacid substitutions were incubated with the DN30 antibody. The complexes were immunoprecipitated with protein A -that binds to the antibody- and revealed with HRP-conjugated streptactin -that binds to the strep-tag in the decoy (left panel). 30 µl of normalized supernatants used for the immunoprecipitation were run on SDS PAGE to verify decoyMET receptors loading (right panel). **(C)** Wild-type decoyMET or decoyMET^{K842E} were incubated with DN30 or DO24 antibodies. The complexes were immunoprecipitated and revealed as in B (left panel). 30 µl of normalized supernatants used for the immunoprecipitation were run on SDS PAGE to verify decoyMET receptors loading (right panel). **(D)** ELISA binding analysis. DN30 mAb (left panel) or DO24 mAb (right panel) were in liquid phase, wild-type decoyMET or decoyMET^{K842E} in solid phase. Antibody binding was detected using an HRP-conjugated anti-mouse antibody. OD, optical density at 450 nm. Each point is the mean of values in triplicate ± SD. **(E)** Homology model of MET IPT 3-4 domains (wild-type and mutated). The structure is displayed in 'stick and ball' mode: IPT 3 yellow, IPT 4 blue. The residues at position 482 (red) are displayed in 'space filling' mode.

Figure 2. DecoyMET^{K842E} binds HGF at high affinity and inhibits HGF-induced MET phosphorylation.
(A) Wild-type decoyMET or decoyMET^{K842E} were incubated with supernatants from cells expressing or not HGF, immunoprecipitated with the anti-MET DO24 antibody and immunoblotted with a biotinylated anti-HGF antibody (upper panel). p90, HGF single-chain precursor; p60, HGF α-chain; p32-p34, HGF β-chain. The same blot was stripped and re-probed with an anti-MET antibody (lower panel). p100, decoyMET. **(B)** ELISA binding analysis. The DO24 anti-MET antibody was used to capture wild-type decoyMET or decoyMET^{K842E} in solid phase; increasing concentrations of HGF were added in liquid phase. HGF binding was detected using a

biotinylated anti-HGF antibody. Each point is the mean of values in triplicate ± SD. **(C)** HGF-induced MET phosphorylation. A549 cells were incubated with wild-type decoyMET or decoyMET^{K842E} (2 μM) and stimulated with HGF (50 ng/ml). Total cell lysates were immunoblotted with anti-phosphoMET (upper panel), anti-vinculin (middle panel) or with anti-MET antibodies (lower panel). p145, mature form of MET; p117, vinculin; p190, single-chain precursor of MET. Heatmaps represent the amount of phosphoMET levels normalized on vinculin measured by densitometry.

Figure 3. MvDN30 and DecoyMET^{K842E} cooperate in reducing HGF-induced MET phosphorylation and MET-driven biological activities.

(A) HGF-induced MET phosphorylation. A549 human lung adenocarcinoma cells were incubated with 2 μM decoyMET^{K842E} , 125 nM MvDN30 or the combination of the two, and stimulated or not with 50 ng/ml HGF. Total cell lysates were immunoblotted with anti-phosphoMET (upper panel), anti-vinculin (middle panel) or anti-MET antibodies (lower panel). p145, mature form of MET; p117, vinculin; p190, single-chain precursor of MET. Heatmaps represent the amount of phosphoMET levels normalized on vinculin measured by densitometry. **(B)** HGF-induced ERK and AKT phosphorylation. A549 human lung adenocarcinoma cells were incubated with 500 nM MvDN30, 2 M decoyMETK842E or the combination of the two, and stimulated or not with 100 ng/ml HGF. Total cell lysates were immunoblotted with anti-phosphoERK, anti-ERK, anti-phosphoAKT, anti-AKT, anti-GAPDH. p42/44, ERK; p60, AKT; p36, GAPDH. Heatmaps represent the amount of phosphoprotein levels normalized on the corresponding total proteins measured by densitometry. **(C)** Anchorage-independent growth sustained by autocrine HGF stimulation. U87-MG human glioblastoma cells, expressing both HGF and MET proteins, were treated with 0.5 μM MvDN30 or 1 μM decoyMET^{K842E}, alone or in combination. Graph represents percentage of average colony growth for each treatment compared to the untreated control. **(D)** Anchorage-independent growth sustained by paracrine HGF stimulation. A549 cells were stimulated with 30 ng/ml HGF and treated with 1μM MvDN30 or 1 μM decoyMET^{K842E}, alone or in combination. Graph represents percentage of average colony growth for each treatment compared to the HGF-stimulated control. **(E)** Transwell invasion assay. HPAF-II human pancreatic adenocarcinoma cells were stimulated with 12.5 ng/ml HGF and treated with 0.5 μM MvDN30 or 1 μM decoyMET^{K842E}, alone or in combination. Graph represents the percentage of invasion in comparison to the HGF-stimulated control. Right panel, one representative

image/group of the cells migrated through the matrigel layer. n.t., not treated cells. Magnification, 200x. Each point is the mean of values in triplicate ± SD. ***= $P \leq 0.001$; **= $P \leq 0.01$; * = $P \leq 0.05$.

Figure 4. MvDN30 and DecoyMET^{K842E} synergize to inhibit HGF-dependent cell scattering.

(A) Analysis of cell motility. HPAF-II cells were pre-incubated with different concentrations (0.06, 0.25, 1 or 4 µM) of MvDN30 or decoyMET^{K842E}, alone or in 1:1 combination, and then stimulated with 6.25 ng/ml HGF. Cell scattering was monitored in real time using an X-CELLigence RTCA device and is expressed as Normalized Cell Index. Each graph refers to one treatment concentration. **(B)** Representative images of HPAF-II cells pre-incubated with 1 µM MvDN30 or 1 µM decoyMET^{K842E}, alone or in combination, and then stimulated with 6.25 ng/ml HGF. n.t., not treated cells. **(C)** Cell motility curve. Effect = Cell index values measured at the end of the experiment for each dose of treatment, normalized on the values obtained with HGF alone and expressed as [1-x]. **(D)** Drug combination analysis. Values from the cell motility curve were elaborated with the Calcusyn software to calculate the Combination Index (CI) for each concentration of MvDN30 and decoyMET^{K842E}. CI = 1, cooperation; CI <1, synergism; CI>1, antagonism.

Figure 5. MvDN30 and DecoyMET^{K842E} in combination strongly impair the growth and survival of patient-derived colon cancer spheroids.

(A) M049 colon spheroids enriched in cancer progenitor cells were pre-incubated with 20 ng/ml HGF and treated with increasing concentrations (0-700 nM) of MvDN30 or decoyMET^{K842E}, alone or in 1:1 combination. The number of viable cells was determined by measuring cellular ATP. RLU, Relative Light Unit. AU, Arbitrary Unit. IC_{50}, Inhibitory Concentration 50. Each point is the mean of values in triplicate ± SD. **(B)** M049 cells were pre-incubated with 20 ng/ml HGF, treated with 77 nM MvDN30 or 25 nM decoyMET^{K842E}, alone or in combination, and processed for apoptosis analysis. Programmed cell death was measured by the free nucleasome method. Each point is the mean of values in triplicate ± SD and is normalized for cell number. Cell death index = free nucleasomes/cell. **(C)** Analysis of phosphoMET status in M049 cells treated with HGF, MvDN30 and decoyMET^{K842E} as in (B). Left panel: representative confocal sections showing anti-phosphoMET in red, DAPI in blue (merged in the top row) and phalloidin in green (bottom row). Graph on the right reports the Mean Fluorescence Intensity (MFI) of phosphoMET,

background subtracted and normalized on phalloidin. Each point is the mean of 5 values ± SEM. Bar is 50 µm. ***= $P \leq 0.001$; **= $P \leq 0.01$; * = $P \leq 0.05$.

Figure 6. MvDN30 and DecoyMET^{K842E} reduce MET phosphorylation and metastatic dissemination of pancreatic cancer cells in hHGF-Ki mice.

Luciferase-expressing HPAF-II cells were injected in the pancreas of hHGF-Ki mice and stratified into four homogeneous groups: VEHICLE (*n*=10), MvDN30 (*n*=6), decoyMET^{K842E} (*n*=6), the combination of the two (*n*=6). **(A)** PhosphoMET status within tumors measured by immunofluorescence. Left panel, representative confocal sections showing anti-phosphoMET in red and DAPI in blue (merged in the top row). Graph on the right reports the Mean Fluorescence Intensity (MFI) of phosphoMET, background subtracted and normalized on DAPI. Each point is the mean of 12 values ± SEM. Bar is 50 µm. **(B)** Evaluation of the EMT phenotype of HPAF-II tumors by immunofluorescence analysis of E-cadherin and vimentin expression. Left panel, representative images of each experimental group. Anti-E-cadherin in green , anti-vimentin in red and DAPI in blue. Bar is 50 m. Magnifications of selected fields are shown in the insets. Bar is 10 m. Graph on the right reports average values obtained by the analysis of 6 images per each tumor ± SEM. EMT phenotype is expressed as Vimentin/E-cadherin ratio. **(C)** Metastatic nodules in the lungs evaluated by histochemical HE staining. Graph on the left: number of metastatic lesions; each point represents the number of lesions scored for each mouse. Graph on the right: area of metastatic lesions; each point represents the average area of metastases measured for each mouse. Ten slides/mouse were analyzed; metastatic lesions were scored and their area quantified with ImageJ. ***= $P \leq 0.001$; **= $P \leq 0.01$; * = $P \leq 0.05$.

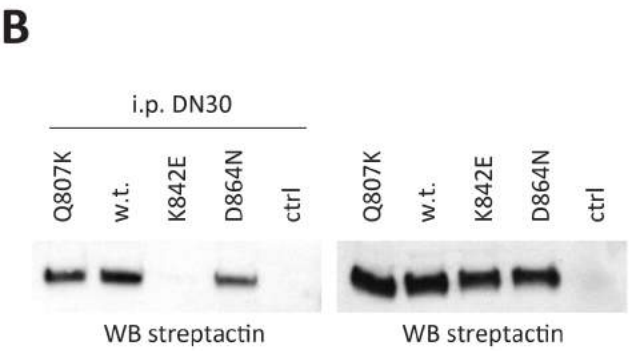

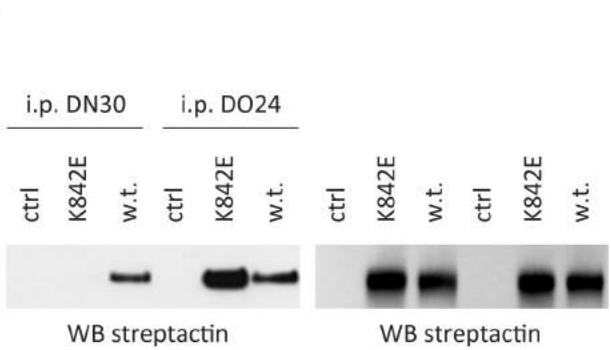

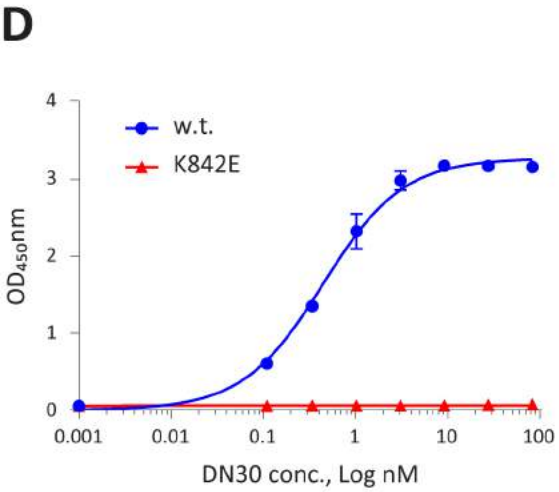

	w.t.	K842E
Kd, nM	0.446 ± 0.027	n.a.

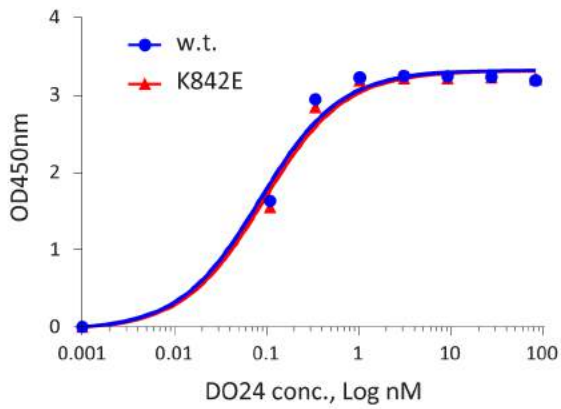

	w.t.	K842E
Kd, nM	0.085 ± 0.009	0.093 ± 0.009

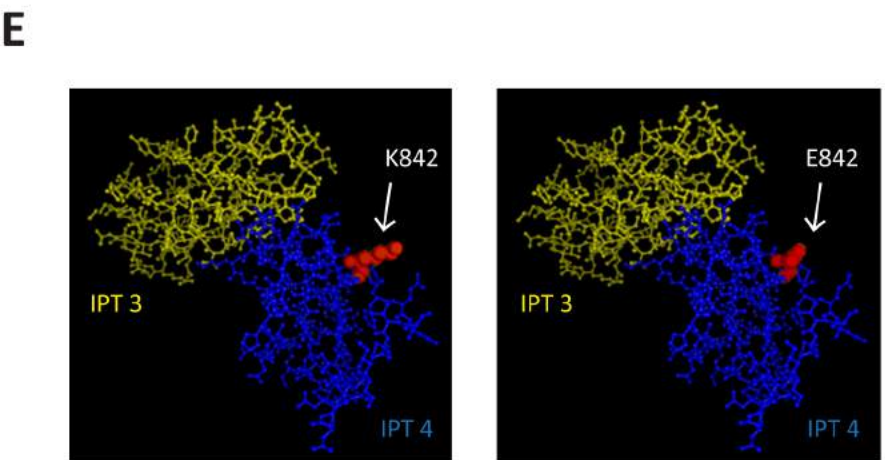

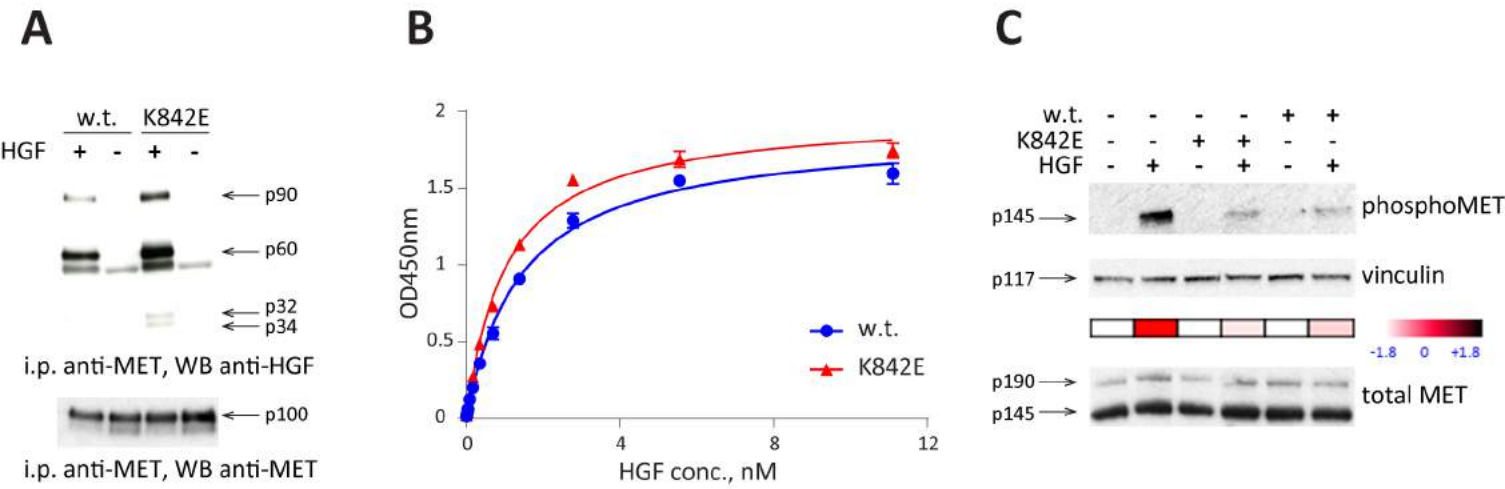
A
w.t.
K842E
HGF + - + -
p90
p60
p32
p34
i.p. anti-MET, WB anti-HGF
p100
i.p. anti-MET, WB anti-MET
B
OD450nm
2
1.5
1
0.5
0
0
4
8
12
HGF conc., nM
w.t.
K842E
C
w.t. - - - - + +
K842E - - + + - -
HGF - + - + - +
p145
phosphoMET
p117
vinculin
-1.8 0 +1.8
p190
p145
total MET

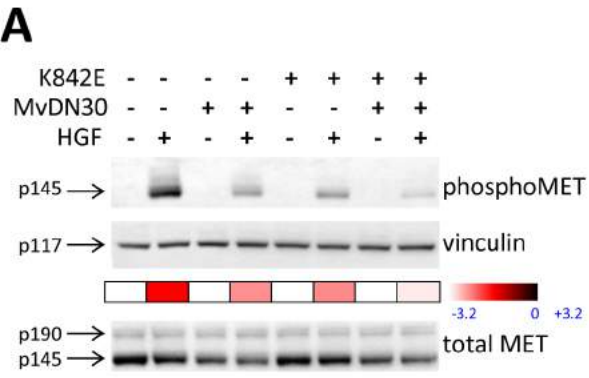
A
K842E - - - - + + + +
MvDN30 - - + + - - + +
HGF - + - + - + - +
p145
phosphoMET
p117
vinculin
-3.2 0 +3.2
p190
p145
total MET

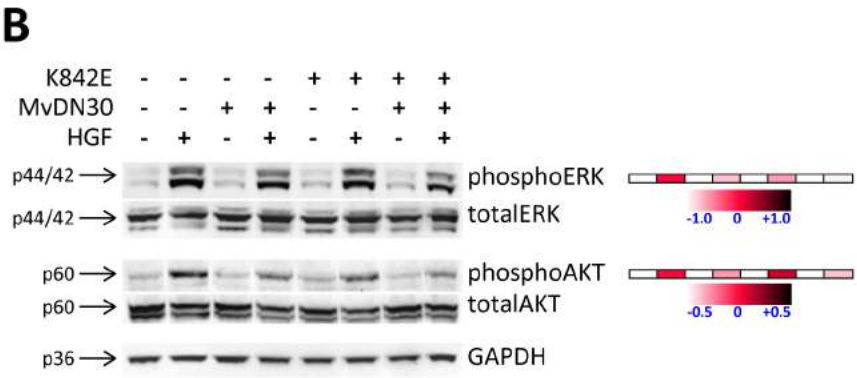
B
K842E - - - - + + + +
MvDN30 - - + + - - + +
HGF - + - + - + - +
p44/42
phosphoERK
p44/42
totalERK
-1.0 0 +1.0
p60
phosphoAKT
p60
totalAKT
-0.5 0 +0.5
p36
GAPDH

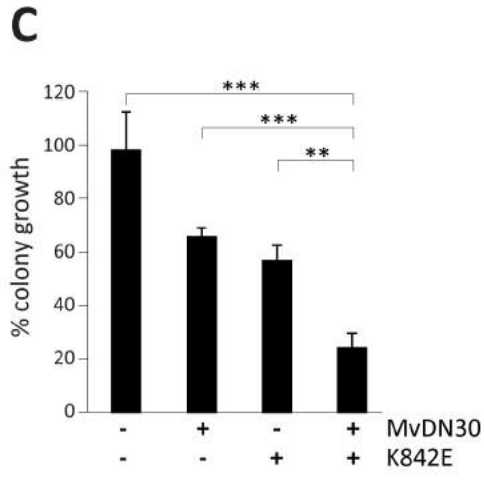
C
% colony growth
120
100
80
60
40
20
0
***
***
**
- + - + MvDN30
- - + + K842E

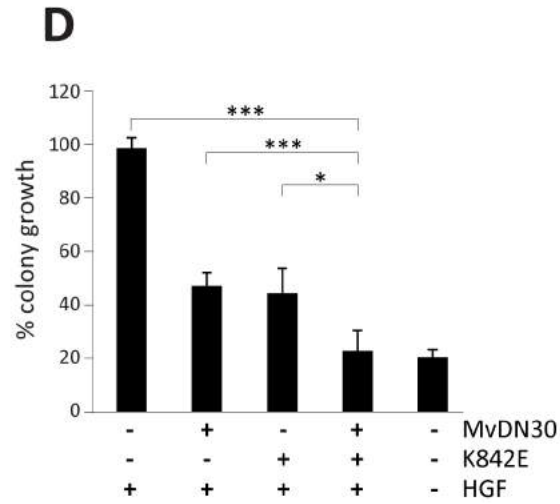
D
% colony growth
120
100
80
60
40
20
0
***
***
*
- + - + - MvDN30
- - + + - K842E
+ + + + - HGF

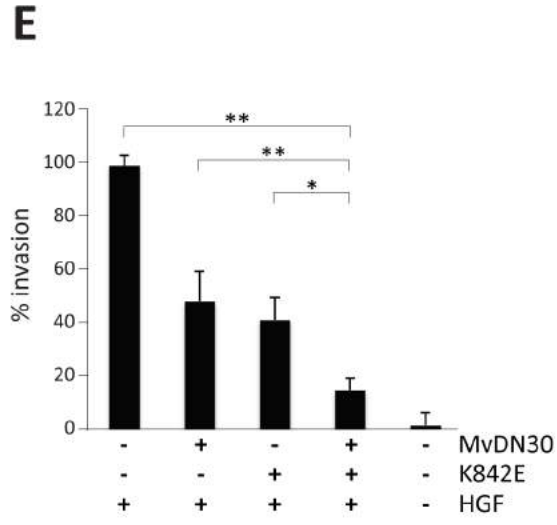
E
% invasion
120
100
80
60
40
20
0
**
**
*
- + - + - MvDN30
- - + + - K842E
+ + + + - HGF

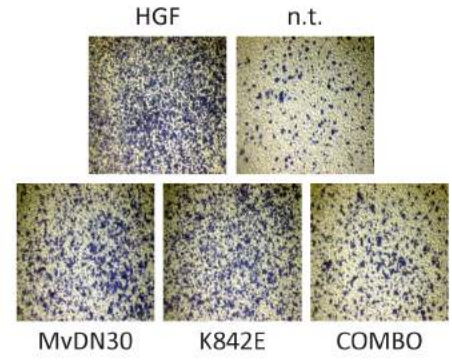
HGF
n.t.
MvDN30
K842E
COMBO

A

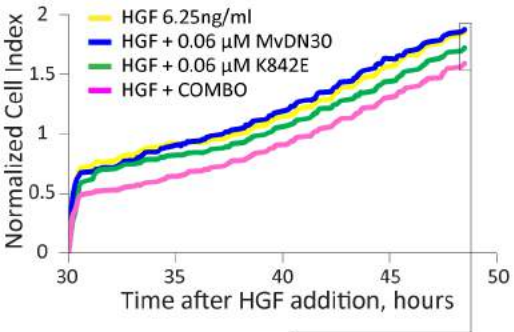

% inhibition	
MvDN30	0
K842E	7.41
COMBO	14.48

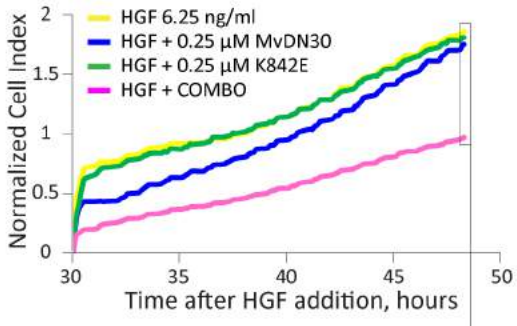

% inhibition	
MvDN30	5.79
K842E	2.69
COMBO	48.19

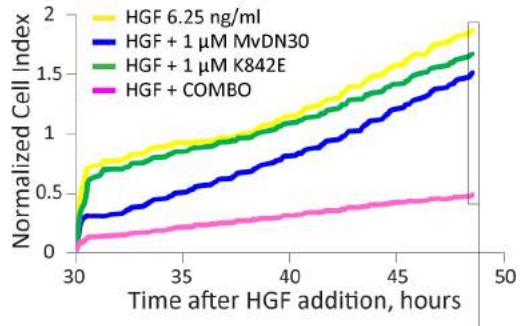

% inhibition	
MvDN30	19.21
K842E	10.50
COMBO	74.52

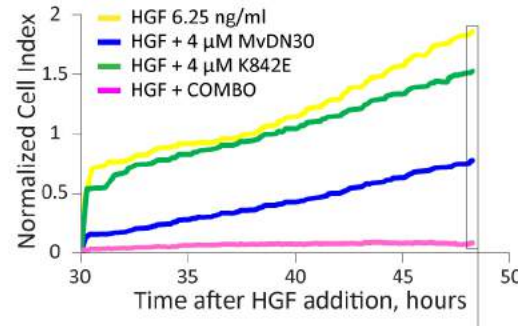

% inhibition	
MvDN30	58.60
K842E	17.88
COMBO	96.04

B

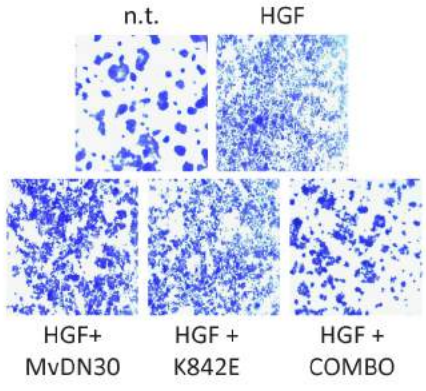

C

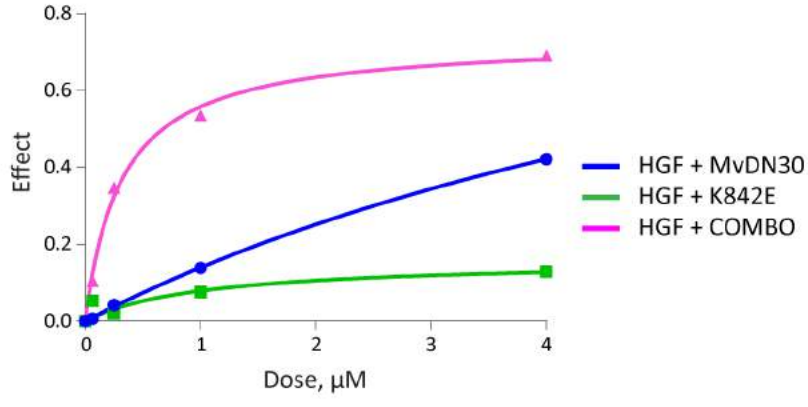

D

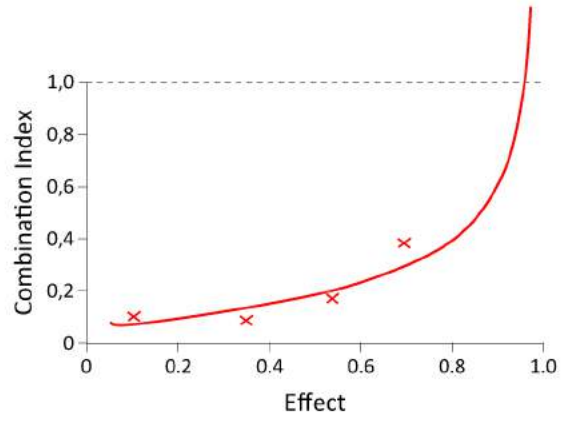

A

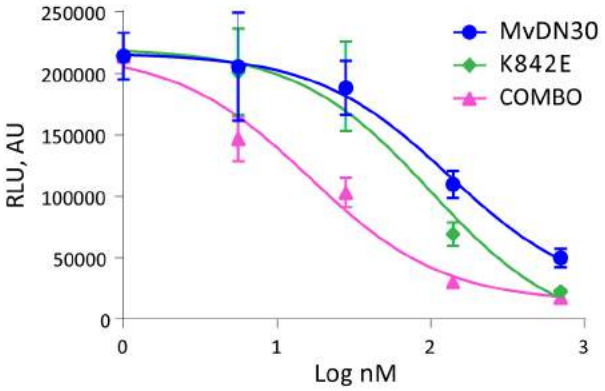

	MvDN30	K842E	COMBO
IC_{50}, nM	131.30 ± 1.43	99.52 ± 1.44	16.28 ± 1.27

B

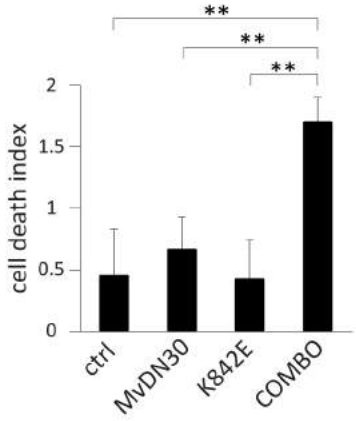

C

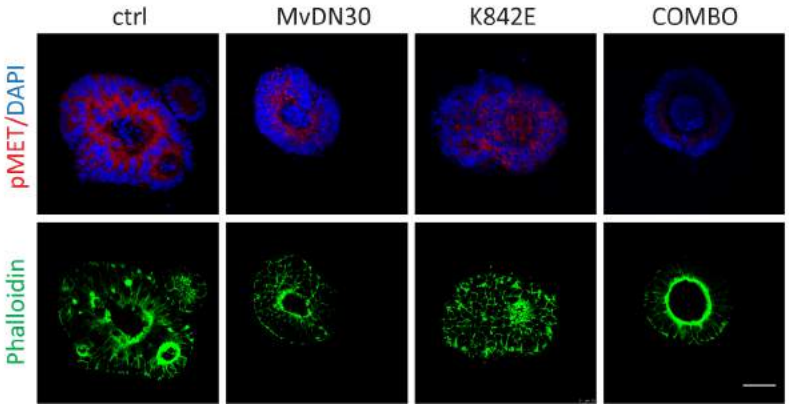

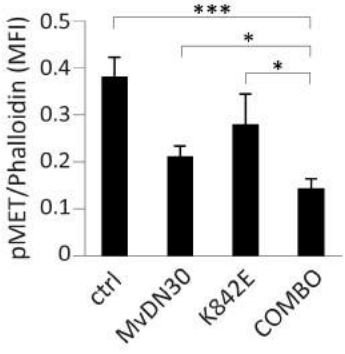

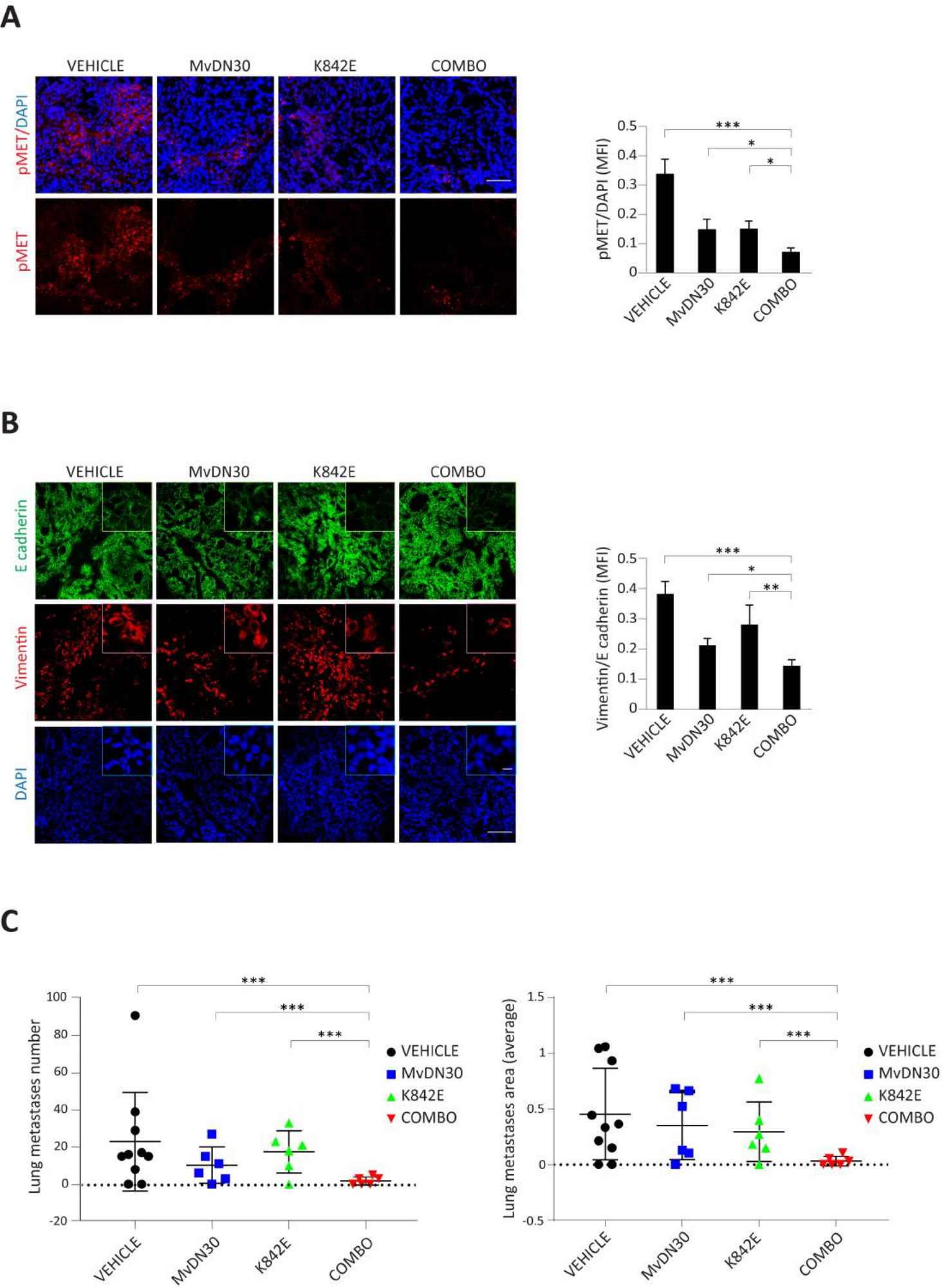
A
VEHICLE
MvDN30
K842E
COMBO
pMET/DAPI
pMET
pMET/DAPI (MFI)
0.5
0.4
0.3
0.2
0.1
0
***
*
*
VEHICLE
MvDN30
K842E
COMBO
B
VEHICLE
MvDN30
K842E
COMBO
E cadherin
Vimentin
DAPI
Vimentin/E cadherin (MFI)
0.5
0.4
0.3
0.2
0.1
0
***
*
**
VEHICLE
MvDN30
K842E
COMBO
C
Lung metastases number
100
80
60
40
20
0
-20
***
***
***
VEHICLE
MvDN30
K842E
COMBO
VEHICLE
MvDN30
K842E
COMBO
Lung metastases area (average)
1.5
1
0.5
0
-0.5
***
***
***
VEHICLE
MvDN30
K842E
COMBO
VEHICLE
MvDN30
K842E
COMBO

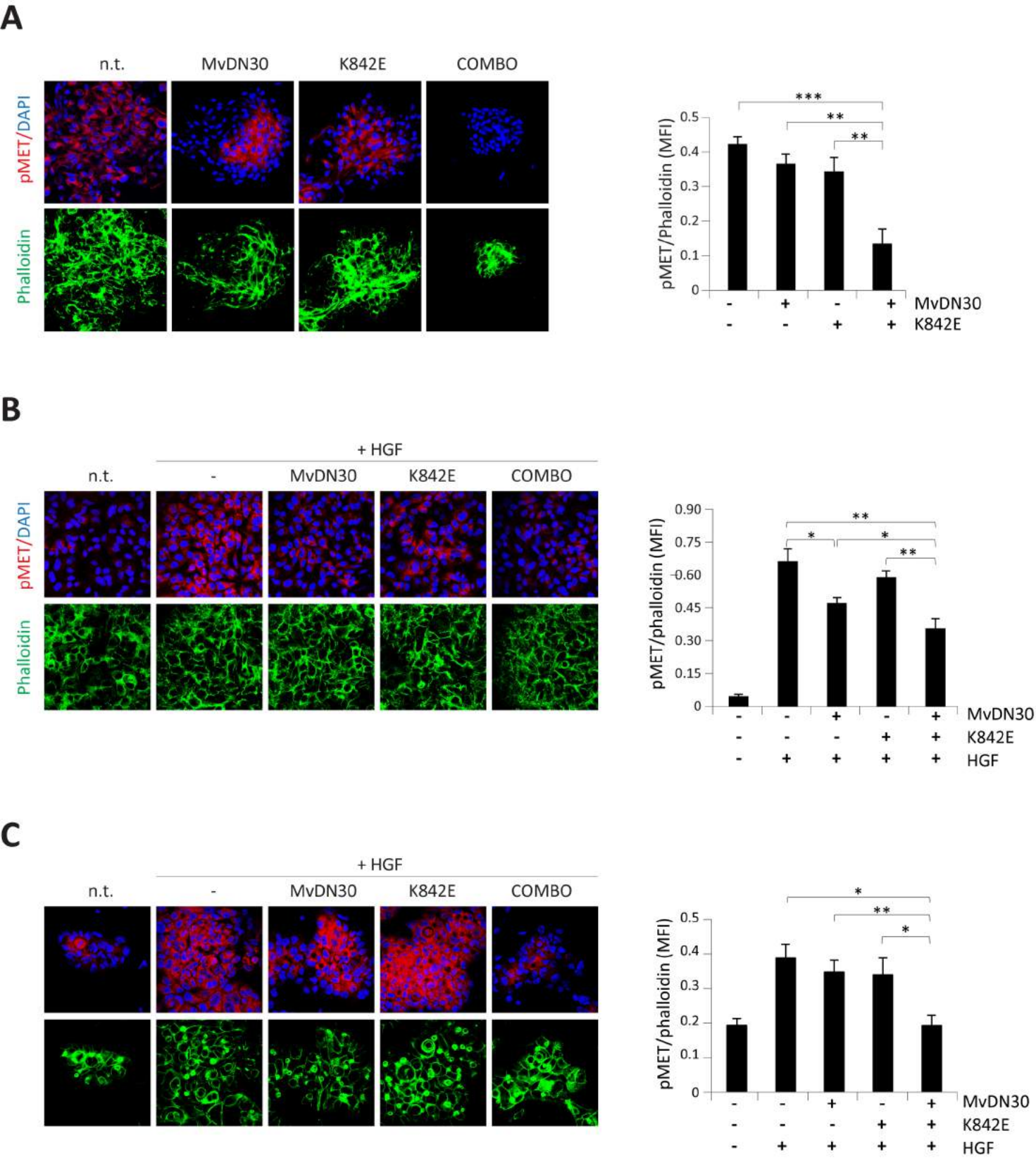

Supplementary Figure 1. MvDN30 and decoyMET^{K842E} in combination inhibit HGF-dependent MET phosphorylation.

U87MG **(A)**, A549 **(B)** and HPAF-II **(C)** cells were treated with MvDN30, decoyMET^{K842E} or the combination of the two (COMBO). HPAF-II and A549 cells were stimulated or not with HGF; n.t., not treated cells. Left panels: representative confocal sections showing anti-phosphoMET in red, DAPI in blue (merged in the top rows) and phalloidin in green (bottom rows). Graphs on the right report the Mean Fluorescence Intensity (MFI) of phosphoMET, background subtracted and normalized on phalloidin. Each point is the mean of 5 values ± SEM. Bar is 50 µm. ***= $P \leq 0.001$; **= $P \leq 0.01$; * = $P \leq 0.05$.

A

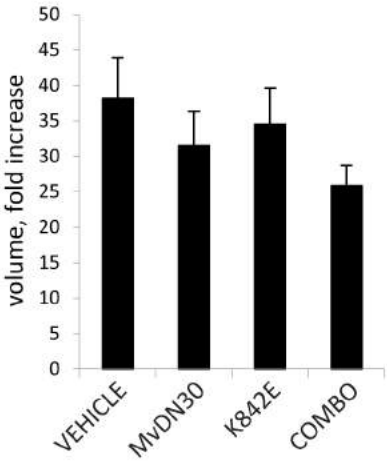

B

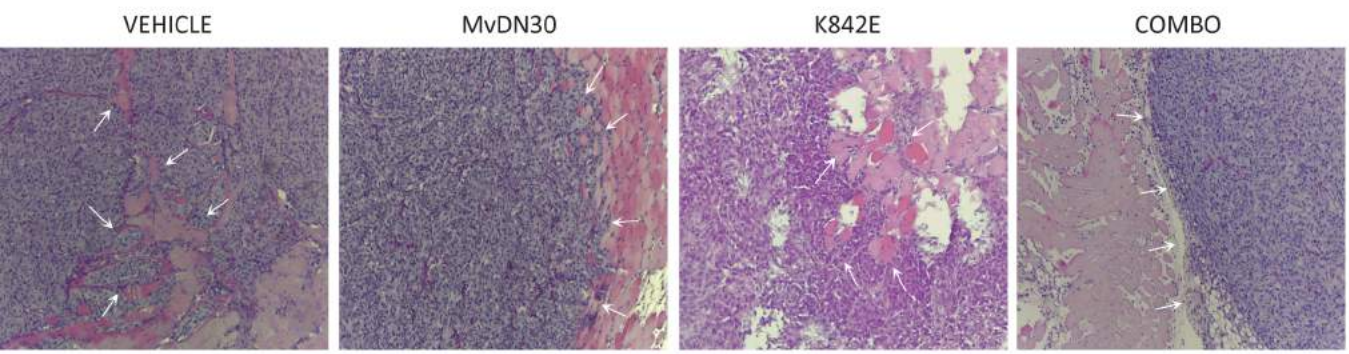

Supplementary Figure 2. MvDN30 and decoyMET^{K842E} in combination reduce the invasive phenotype of subcutaneous U87-MG tumors.

U87-MG cells were injected subcutaneously in NOD-SCID mice. When the tumors reached a volume of 80-100 mm^3, mice were stratified in four homogeneous groups: VEHICLE (*n*=10); MvDN30 (*n*=9); K842E (*n*=9); the combination of the two (*n*=10). **(A)** Tumor volume at sacrifice, expressed as fold increase. Each bar is the mean of the group ± SEM. Differences among the groups are not statistically significant. **(B)** Histochemical analysis of tumor burden. Representative images of hematoxylin-eosin stained tumor sections. Arrows point to the boundary between the tumor and the surrounding tissue. Magnification 100x.

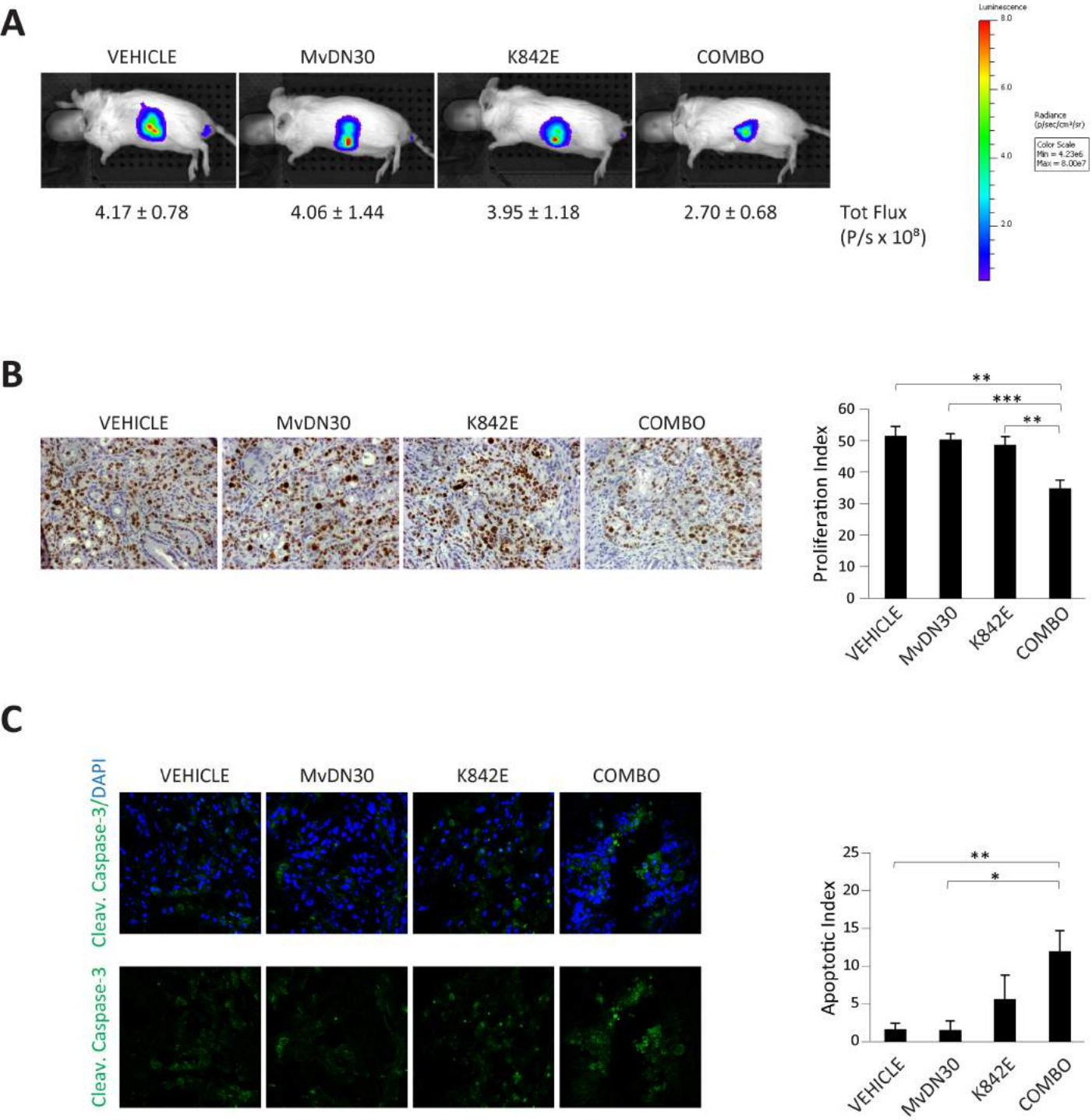

Supplementary Figure 3. Effect of MvDN30 or decoyMET^{K842E}, alone and in combination, on the proliferation and apoptosis of pancreatic cancer cells injected orthotopically in hHGF-Ki mice.

hHGF-Ki mice injected with luciferase-expressing HPAF-II cells were stratified in four homogeneous groups: VEHICLE (*n*=10), MvDN30 (*n*=6), decoyMET^{K842E} (*n*=6), a combination of the two (*n*=6). **(A)** Tumor bioluminescence detected by IVIS Spectrum. Images show one representative mouse per group. Numbers indicate the average values of total flux of bioluminescence (photons/second x 10^8) of each experimental group ± SEM. Differences among the groups are not statistically significant. **(B)** Analysis of tumor cell proliferation measured by Ki67 immunohistochemistry. Left panel, representative images of each experimental group. Magnification, 200x. Graph on the right reports average values obtained by the analysis of five images per tumor ± SEM. Proliferation Index is calculated as Ki67 positive cells/total number of cells. **(C)** Analysis of tumor cell apoptosis measured by cleaved Caspase-3 immunofluorescence. Left panel, representative images of each experimental group. Anti-cleaved Caspase-3 in green, DAPI in blue (merged in the top row). Bar is 50 µm. Graph on the right reports average values obtained by the analysis of 8 images per tumor ± SEM. Apoptotic index is calculated as cleaved Caspase-3 positive cells/total number of cells. Bar is 50 µm. *** = *P* value < 0.001; **= *P* value < 0.01; *= *P* value < 0.05.